G. Testa, G. Persichetti and R. Bernini, "Hollow-Core-Integrated Optical Waveguides for Mid-IR Sensors," in IEEE Journal of Selected Topics in Quantum Electronics, vol. 24, no. 6, pp. 1-8, Nov.-Dec. 2018, Art no. 5700108, doi: 10.1109/JSTQE.2018.2818465.

Hollow-core integrated optical waveguides for Mid-IR sensors

Genni Testa, Gianluca Persichetti, and Romeo Bernini

***Abstract*—Integrated hollow-core antiresonant reflecting optical waveguides are designed and analyzed for mid-infrared propagation. With a proper selection of waveguide materials and geometry, low loss propagation lower than 1.5 dB/cm in the whole 2.5-14 µm range could be achieved. Single mode waveguides, with a modal purity above 95% after propagation lengths of few millimeters, have been designed at 4µm and 9µm. The waveguides could be realized using fabrication and materials fully compatible with standard Silicon technology, enabling the chip-scale integration of Mid-IR devices for gas sensing applications.**

***Index Terms*—Optical waveguides, Integrated optics, Infrared measurements, Spectroscopy.**

I. INTRODUCTION

Mid-infrared (MIR) optical spectroscopy approaches are recognized as very powerful techniques that promise higher sensitivity, specificity, and faster time response for gas and vapour sensing. In fact in this spectral region (2.5-20 µm) resides the characteristic absorption lines of most molecules that provide an unique "fingerprints" that give chemical and compositional information on sample under analysis [1]. However, the implementation of these techniques in compact and portable systems is severely limited by the miniaturization, and high sensitivity optical gas sensors remain traditionally restricted to bulky laboratory equipments.

One of the main challenges towards the implementation of MIR gas sensing in chip formats is the fabrication of low loss optical integrated waveguides [1]. This objective restricts the choice of the materials and related technologies to build optical components, preferably, by using Silicon compatible process [3]. In fact, for instance, while Silicon is transparent in the wavelength range of ~2-8 µm, Silicon Dioxide is lossy in most parts of the MIR spectrum, thus limiting the wavelength range of applicability of the traditional Silicon on insulator (SOI) platform to ~ 1-4 µm. Transparent materials that allow implementing many optical functions over the complete MIR range are required to unlock a broad range of applications. In order to have access to the MIR wavelength range, alternative materials and designs have been explored based on Silicon-on-Sapphire (SOS) [4]-[6], Silicon-on-Nitride (SON) [7]-[9] and Germanium-on Silicon platforms (GOS) [10], [11] as well as air-cladding Silicon pedestal [12], [13] and suspended structures [14]. Another alternative for the realization of planar MIR devices is to use chalcogenide materials [15], [16]. By implementing these design approaches, low-loss waveguides and other interesting passive components operating in the MIR have been fabricated [3], [17], [18]. However, these devices remain not competitive in terms of sensitivity as compared with those operating in the visible-near IR spectral range for liquids sensing, as to why they have not been as largely adopted for gas sensing.

A further obstacle to the chip-scale integration of MIR sensing systems is the weak light–matter interaction typical of gas/vapour samples, when conventional solid core waveguides are used, that causes a low sensitivity. In fact, in these waveguides, only the evanescent tail of the propagating modes penetrates in the outer medium with strong limitations on the partial sensitivity P_p, quantified as the ratio between the optical

Manuscript received February 31, 2018. This work was supported in part by the project IAMICA (I High Technology Infrastructure for Environmental and Climate Monitoring— PONa3_00363). G. Testa, R. Bernini and G. Persichetti are with the Institute for electromagnetic sensing of the environment (IREA), Napoli, Italy (persichetti.g@irea.cnr.it, bernini.r @irea.cnr.it, corresponding author to provide e-mail: testa.g@irea.cnr.it).

power fraction in the sensing material P_s to the total mode power P_{tot} ($P_p=P_s/P_{tot}$). In order to increase the sensitivity, the waveguide size has been reduced up to nanometric scale [19] and using Silicon slot waveguides partial sensitivity of 0.58 has been obtained [20]. However, their fabrication can be very challenging as well as the fiber-to-waveguide optical coupling.

Based on these considerations, hollow core waveguides (HCWs) are promising candidates to overcome the aforementioned limitations, as they intrinsically provide, throughout the waveguiding structure itself, a hollow cavity that can serve as micro channel for gas flowing [21]-[23].

Due to the huge potential the HCWs have to act as vessels for gases, the basic idea to exploit this sensing strategy in the field of gas sensing started to gain attention since the first introduction of the photonic band-gap fibers, quickly adapted from telecommunication applications, for which they were originally developed, to gas sensing [24], [25]. However, hollow waveguides in the form of optical fibers or capillary structures have a limited range of applicability to only use as long path length gas cells, resulting often in cumbersome sensor configurations, which suffer from mechanical instability and require very careful handling.

Recently, the first example of substrate-integrated metallic HCWs has been proposed, enabling to narrow the existing gap between the enormous potential offered by HCWs and their practical implementation in a robust and compact MIR device for gas sensing [26], [27]. The device exploits metallic HCWs in spiral-type waveguide channel geometry as long pathlength gas cell to increase the sensitivity in MIR absorption spectroscopy. Nevertheless, although this approach offers significant advantages over the evanescent field sensing, it suffers from a limited sensitivity that is typical of single pass absorption. In order to increase the pathlength without increasing the device size, the light may travel through the sample for long time, for instance by using optical cavity design instead of the single-pass waveguide geometry. However, the multimode propagation in metallic HCWs could lead to problems associated with the so called “modal noise” [ref?]. Thus, their function remains largely restricted to use as high efficient long path gas cells, which basically benefit of an enhanced partial sensitivity.

In this paper we propose ntiresonant reflecting optical waveguides (ARROWs) as low loss single mode waveguides in the MIR between 2.5-14 µm. ARROWs have found a growing interest for their use as basic element in chip-scale sensor devices in the field of optofluidics for fluid sensing in the visible spectral range [28], [29]. High sensitivity has been demonstrated in ARROW-based devices by exploiting the direct interaction of the entire optical waveguide mode with liquid samples [30], [31]. Such a strong optical coupling, combined with ultra-small liquid volume, has enabled sensitivity down to single molecule detection, which is the ultimate goal of analytical methods [29], [32]. We believe that ARROWs with hollow core have an analogous potential in the field of MIR optical sensing of gases/vapours. In a previous work, multimodal hollow core ARROW with hexagonal cross section and operating in the visible range have been reported [33]. In this work, two waveguide geometries have been designed and analyzed for single mode operation in MIR spectral range, and the influence of the fabrication materials on the optical losses has been evaluated. The results of the analysis and the numerical simulations show that low loss single mode ARROWs could be fabricated by using material compatible with conventional Silicon planar technologies. These waveguides could be used as building blocks in high performances devices, as optical resonators [34], for high sensitivity gas detection.

II. ARROW WAVEGUIDES DESIGN

The light confinement in ARROW waveguides is achieved by a highly reflectivity mirror produced by a multilayer stack of alternating high and low- refractive index cladding layers. Light propagates through the core by means of multiple Fresnel reflections at the cladding interfaces, each cladding layers being designed to act as a Fabry–Perot cavity in antiresonance condition. The reflectivity of the mirror resulting from multiple interference claddings can be very high, up to 99%. One possible ARROW structure for both vertical and horizontal confinement is illustrated in Fig. 1a). In this layout the core must be completely surrounded by the solid cladding layers (SC-ARROW) to accomplish light-confinement in both lateral and vertical direction [30]. In addition to this conventional structure, we also analyse a hybrid Solid/Hollow claddings ARROW (SHC-ARROW) [35], as depicted in Fig. 1b). In this hybrid version, the vertical confinement is achieved by a multi-layered structure made up of solid claddings, while lateral confinement is achieved by employing alternating solid/hollow cladding. Although this configuration is very promising, it has practically remained unexplored [36].

The optimal thickness of the cladding layers can be derived taking into account the phase accumulated by the fundamental mode at each round trip in the interference claddings and setting the specific condition of antiresonance [35]:

$$d_i = \frac{\lambda}{4}\frac{\{(2N+1)+[(\phi_{1,i}+\phi_{2,i})\bmod(2\pi)/\pi]\}}{\sqrt{1-\left(\frac{n_c}{n_i}\right)^2+\left(\frac{\lambda}{2n_i d_c}\right)^2}} \quad N=0,1,2,... \quad (1)$$

here λ is the working wavelength, d_c is core size, n_c is the core refractive index, n_i is the refractive index of the cladding layers i and $\phi_{1,i}$ and $\phi_{2,i}$ are the phase shifts at both interfaces of layer i. Typically, the sum of $\phi_{1,i}$ and $\phi_{2,i}$ is a multiple of 2π, resulting in quarter-wavelength cladding stack. However, in ARROW waveguides with gaseous core, the reflection angle at first cladding layer for TM modes could exceed Brewster's angle. In this case the sum of the phase shift is an odd multiple of π, resulting in a thickness of the first cladding layer proportional to an half-wavelength. Both configurations could be fabricated by standard bulk micromachining process. The ARROW is constituted by two halves of silicon substrates with the core etched in one of the halve part. The two processed silicon substrates are finally bonded after cladding depositions on both halves.

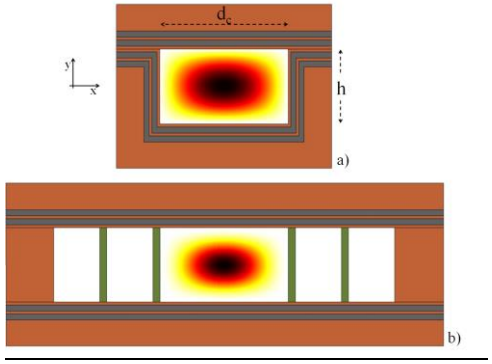

Fig.1. Schematic layout of the a) SC-ARROW and b) SHC-ARROW waveguide with two bilayers with intensity profile of simulated fundamental quasi TE-modes at the wavelength of λ=4μm with waveguide parameters of d_c=12λ and h=7λ.

About waveguide material selection, in conventional solid core waveguides this choice is essentially dictated by the material losses, that limit the overall performances of the structure. In hollow core ARROWs this choice is trickier, because of the leaky nature of these waveguides. In fact, the interferometric confinement mechanism in the cladding layers is strongly influenced by both real and imaginary part of cladding material refractive indexes. In particular, the cladding material losses have two noticeable effects. First, it causes a direct increase of optical losses due to the light absorption in the cladding layers, which in turn causes an increase of the propagation losses. The second effect is a decrease of the cladding reflectivity because the absorption in the first layers masks the outer claddings to the core modes [37]. This means that the light which escapes the core is absorbed before it can be reflected back into it and therefore, the internal cladding becomes equivalent to an infinite cladding.

As concerning the real part of the refractive index, for a simple one dimensional slab ARROW with only one bilayer cladding, a simple analytical expression given in [37] permits to calculate the ARROW attenuation coefficient for the TE and TM fundamental modes in the following, very useful, approximated form [30]:

$$\begin{cases} \alpha_{TE} = \dfrac{\lambda^4\left[1+\dfrac{4d_c^2}{\lambda^2}\left(n_2^2-n_c^2\right)\right]}{4n_c d_c^5\left(n_1^2-n_c^2\right)\sqrt{\left(n_s^2-n_c^2\right)}} \\ \alpha_{TM} = \left(\dfrac{n_1^2 n_s}{n_c n_2^2}\right)^2 \alpha_{TE} \end{cases} \quad (2)$$

Equation (2) indicates that the TE losses strongly depend upon on the refractive index differences between the core and the first cladding, and the core and the second cladding. Thus far, in order to minimize the TE losses, two requirements on cladding materials refractive indexes are needed:

1) the refractive index of the first cladding must be much higher than the core index ($n_1 > n_c$)
2) the refractive index of the second cladding should be as near as possible to the core index ($n_2 \approx n_c$).

However, Eq. (2) shows also that the optimization of TE losses induces a high loss discrepancy between TE and TM losses due to the large difference of refractive indices between core (n_c) and the first cladding layer (n_1), and also between the first cladding (n_1) and the substrate (n_s). Hence, the simple rule of using bilayers with the higher index-contrast is not always the better choice to minimize the losses for quasi-linearly polarized modes [35]. In particular, this rule does not apply for TM polarization. Moreover, if the vertical and horizontal cladding materials are the same, from Eq. (2) TE

losses are always lower as compared with TM. For this reason, the propagation of TE polarized mode is often preferred due to typical lower attenuation coefficients.

This one-dimensional analysis could be extended to a bi- dimensional geometry by using a paraxial approximation. In this case, the problem of the 2-D ARROW confinement can be separated into two 1-D problem for the lateral and transverse direction, in this way the evaluation of the total losses can be obtained from the addition of the resulting 1-D losses [38]. In particular, if incident light is polarized along x axis (Fig. 1) it is reflected upon lateral cladding as TM-polarized light whereas it is TE-polarized with respect to the vertical ARROW confinement. Hence, TE polarized input light along x-axis will also contribute to the total losses as a TM polarization with respect to y-axis. This means that the influence of the polarization losses should be taken carefully into account in the waveguide design and could be used in order to obtain waveguides with low loss for linearly polarized propagating modes. Because the TM- component of the losses are typically higher than TE-, the core should be generally wider along the TM polarization direction to minimize this contribution and decrease the waveguide loss (Fig.1).

In the following we present ARROW materials and geometry in order to obtain low loss quasi-TE mode polarized along x axis.

In Fig. 2 and 3 the real and the imaginary part of the most common Si-compatible materials are reported in the range 2.5-14 μm [39].

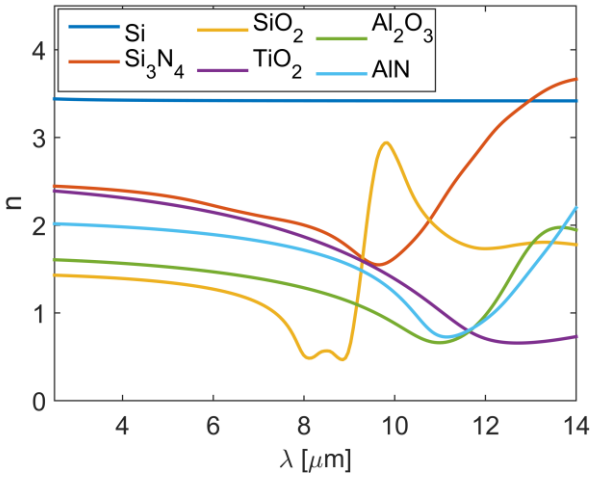

Fig.2. Real parts of the refractive indexes of the considered Si-compatible materials.

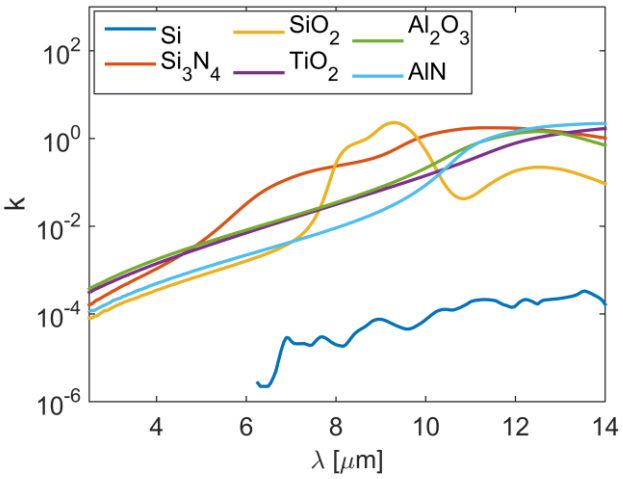

Fig.3. Imaginary parts of the refractive indexes of the considered Si- compatible materials.

As concerning the SC-ARROW waveguide, the materials selection is a compromise between the above requirements for minimizing TE and TM component of the losses. Equation 2 suggests that the best material for the first cladding is Silicon that offers very high refractive index and low losses, whereas Silicon Dioxide, Aluminium Nitride and Aluminium Oxide could be suitable for the second cladding, depending on the MIR wavelength range.

Regarding the SHC-ARROW waveguides, this geometry permits to select different cladding materials for left and right lateral claddings (TM polarization) with respect to the top and bottom vertical claddings (TE polarization). The last ones could be selected analogously to SC-ARROW in order to maximize the refractive index contrast. Instead, for left and right claddings, alternating solid and hollow (Air) claddings are also allowed. Since this configuration allows to satisfy

the condition $n_2=n_c$, it can provide a strong reduction of the TM-component of the losses. As concerning the higher index lateral cladding, the maximum TM reflectivity is obtained for $n_1=\sqrt{2}n_{eff}$ [35], which is around 1.4 for typical values of n_{eff}=0.99.

III. ARROW WAVEGUIDE MIR ATTENUATION

In order to evaluate the performances of the ARROW waveguide in the whole MIR range (2.5-14 μm), the attenuation of the fundamental mode for both SC- and SCH-ARROW geometries with several cladding materials has been calculated.

Assuming an incident light polarized along x axis and taking into account the above considerations on optical losses, a rectangular hollow waveguide geometry has been selected with width $d_c=12\lambda$ and height of $h=5\lambda$. This core size allows low loss propagation of modes polarized along the x-axis (quasi-TE modes). The thickness of cladding layers has been fixed according Eq. (1) with N=0 with the exception of the high index lateral cladding of the SCH-ARROW where N=1 has been used.

The attenuation coefficients of TE and TM fundamental mode have been calculated by ray-optic method taking into account the reflectivity $R_{TE,TM}$ of the dielectric claddings surrounding the core according to the expression [40]:

$$\alpha_{TE,TM}=\frac{\left[1-R_{TE,TM}\right]}{w}\tan(\theta_{TE,TM}) \qquad (3)$$

where $\theta_{TE,TM}$ is the incident angle of the fundamental mode and w= d_c, h for TE- and TM-reflection, respectively.

In Fig. 4 the losses for the fundamental mode of SC-ARROW with two bilayers of different cladding materials are reported. As it can be observed, the combination Si/SiO_2 offers the best performance in the range 2.5-6 μm and 11-14 μm. In the range 6-11 μm both Si/AlN and Si/Al_2O_3 could be used, depending on the operating wavelength.

It is important to underline that in this configuration the optimized thickness of the first lateral cladding is double with respect to the horizontal one due to a phase shift at cladding interfaces (see Eq. (1)).

In Fig. 5 the losses for the fundamental mode of SHC-ARROW with two bilayers of different cladding materials are reported. The combination Si/SiO_2-Si/Air offers the best performance in the range 2.5-8 μm and 11-14 μm. In the range 8-11 μm both Si/AlN-Si/Air and Si/Al_2O_3-Si/Air could be employed.

As discussed in the above section, the maximum TM reflectivity is obtained for $n_1\approx1.4$, which is close to the refractive index of SiO_2 in the 2.5-6 μm range. Hence, despite SiO_2 become lossy above 4 μm, the high TM-reflectivity led to choose SiO_2 as first lateral cladding material, at least up to 6 μm.

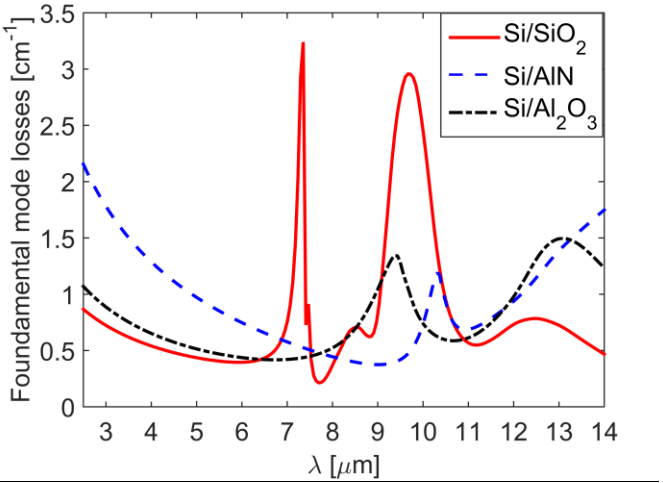

Fig.4 Losses for the fundamental quasi-TE mode for an SC-ARROW waveguide with two bilayers.

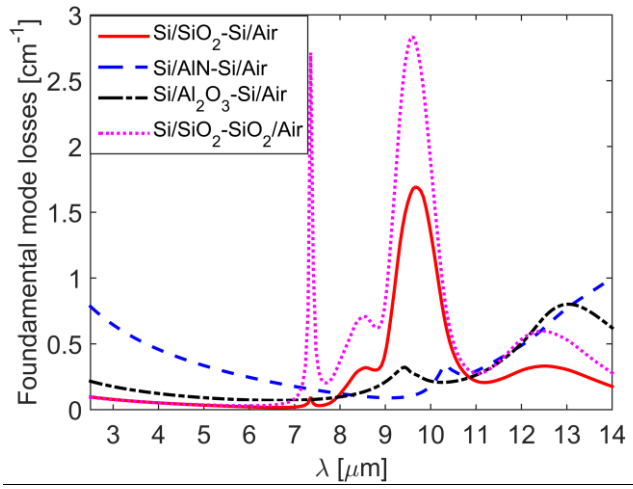

Fig.5 Losses for the fundamental quasi-TE mode for an SHC-ARROW waveguide with two bilayers.

As it can be noticed, in the range 2.5-6 μm the optical losses are comparable with Si/SiO_2-Si/Air, whereas above 6 μm the performance of Si/SiO_2-SiO_2/Air structure become worse. This is due to the SiO_2 absorption, that, as the number of cladding bilayers increases induce a strong increase of the losses. The peak at around λ=10μm in Figs. 4 and 5, for the Si/SiO_2 case, is caused by the decreasing of the cladding refractive index contrast due to the strong increase of the refractive index of the SiO_2 at this wavevelength. Instead, the other pronounced peaks that occur in Figs.4 and 5 are explained by the fact that at some wavelengths, due to the materials dispersion, the incident angle at the first/second cladding interface approaches the Brewster angle, causing a strong reduction of TM reflectivity of the lateral claddings.

By comparing Fig.4 and Fig.5 we can observe that a strong improvement can be obtained with the SHC-ARROW. In particular, in the range 2.5-8 μm the mode attenuations are reduced of a factor around 10, 5 and 2.7 in comparison to SC-ARROW with SiO_2, Al_2O_3 and AlN, respectively. Above λ=8 μm the improvement gradually reduces due to the increase of all materials losses.

These results show that both configurations are very promising for the realization of low loss optical waveguides in the MIR. In particular, with a proper selection of cladding materials, SC-ARROWs allow propagation losses lower than 3.8 dB/cm in the whole range of 2.5-14 μm. Instead, SHC-ARROW enable losses lower that 1.5 dB/cm in the same range, with very low values (0.4 dB/cm) in the 2.5-8 μm interval. These values are comparable or even lower to that of conventional solid core waveguides [19]. However, in comparison, ARROWs offer several advantages like high partial sensitivity (≈1) and large core size that simplify the optical coupling and reduce the coupling losses. Furthermore, concerning the fabrication compatibility, these waveguides require only materials capable of being integrated with Si-CMOS fabrication processes [41].

The above performances have been obtained with only two cladding bilayers. The attenuation could be further reduced as far as the number of bilayers cladding increases (Fig. 6).

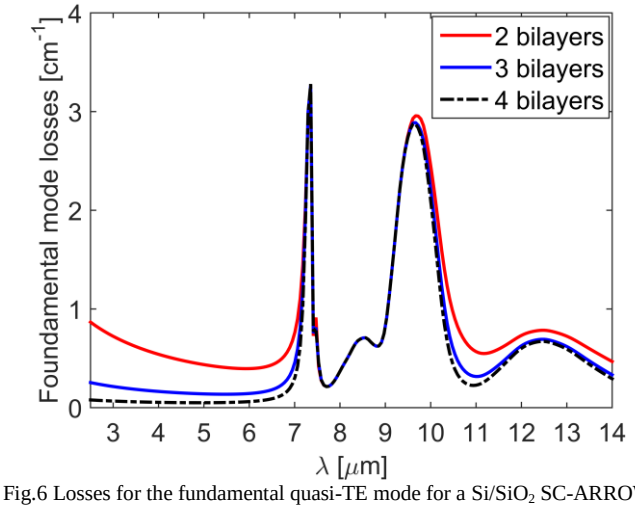

Fig.6 Losses for the fundamental quasi-TE mode for a Si/SiO_2 SC-ARROW waveguides with two, three and four cladding bilayers.

As it can be observed, the loss of Si/SiO_2 SC-ARROW with four bilayers became comparable with the loss of Si/SiO_2-Si/Air SHC-ARROW in the range 2.5-7 μm. Above λ=7 μm the absorption of the first SiO_2 layer masks the outer claddings to the core modes, and the loss reduction became negligible.

IV. SINGLE MODE ANALYSIS OF SC-ARROW

In this section, we report on the design criteria to obtain single mode operation of the waveguide. This is of particular importance as single mode ARROWs could be used to shape many of the common building blocks of photonic circuits like low loss straight and curved waveguide sections, multimode interference power splitters [42], interferometric devices like optical ring resonators [34] and Mach-Zehnder interferometers [43], which have been recently demonstrated with liquid core ARROWs in the visible range. Modal analysis of the SC-ARROW waveguide and SHC-ARROW has been performed with a two dimensional mode solver [FIMMWAVE, ©Photon Design] by using the finite difference method (FDM). In particular, two working wavelength of λ=4, 9 μm have been explored. Depending on the operating wavelength, different cladding materials have been chosen according to the results reported in the above section.

A. Solid cladding ARROW @4micron

From Fig. 4, the best performance at the operating wavelength of λ=4 μm are provided by the Si/SiO_2 material composition for the cladding layers.

In particular, SC-ARROW with two bilayers has been simulated by varying the core width d_c and height h. Simulations have been performed to evaluate the attainable attenuation losses in single mode operation. The core size parameters considered in the simulations are d_c =10λ, 12λ and 14λ and h=3λ, 5λ and 7λ. The appropriate cladding layer thicknesses d_1 and d_2 have been calculated by using Eq. (1) with N=0 for each fixed core width d_c. In Table I and II are summarized the attenuation losses α_0 and the coupling coefficient c_o to the fundamental quasi TE-mode by varying d_c and h. Results of Table I are consistent with results shown in Fig. 4. For the evaluation of the coupling coefficients of Table II, we have used a three dimensional eigenmode expansion method (EME). In the simulations, a single mode fiber at λ=4 μm with a mode field diameter ($1/e^2$) of about 15 μm is considered as input.

TABLE I

FUNDAMENTAL MODE LOSSES α_0[CM^{-1}]

h / d_c	3λ	5λ	7λ
10λ	1.19	0.92	0.88
12λ	0.79	0.56	0.52
14λ	0.59	0.37	0.33

Fundamental quasi TE-mode attenuation losses for different core size (d_c, h) for Si/SiO_2 SC-ARROW waveguides with two bilayers.

TABLE II

COUPLING COEFFICIENTS C_0

h / d_c	3λ	5λ	7λ
10λ	0.63	0.78	0.81
12λ	0.58	0.72	0.75
14λ	0.53	0.66	0.69

Coupling coefficient c_o to the fundamental quasi TE-mode for different core size (d_c, h) for Si/SiO_2 SC-ARROW waveguides with two bilayers.

From Table I it can be noticed that the losses are more affected by the core width d_c, whereas they are less sensitive to the core height h. This behaviour can be explained by considering that the width impacts predominantly on the TM-component of the losses, which constitutes the main contribution of the losses.

As ARROW is a leaky waveguide, in order to evaluate the modal behaviour, attenuation losses of the higher order modes need also to be taken into account in designing a single mode waveguide. Since higher order

modes experience higher losses due to lower reflection coefficients at the cladding interfaces, the optimization of core dimension of a single mode ARROW is a compromise between low fundamental mode attenuation constant and higher order modes filtering effect. The attenuations and the coupling coefficients of all the relevant propagating modes (i.e. with coupling coefficients greater than 0.001%) have been calculated by varying the core width d_c and the height h. The simulation results are summarized in Table III and IV in the case of h=5λ. Propagating modes which couple to less than 0.01% of the input power are not listed in the tables.

TABLE III
MODE ATTENUATION LOSSES $\alpha_0[CM^{-1}]$

dc	α_0	α_{31}	α_{51}
10λ	0.92	7.64	19.82
12λ	0.56	4.52	11.94
14λ	0.37	2.90	7.72

TABLE IV
COUPLING COEFFICIENTS

dc	c_0	c_{31}	c_{51}
10λ	0.78	0.09	0.02
12λ	0.72	0.14	0.03
14λ	0.66	0.17	0.04

From the results is clear that only a small portion of the input power is coupled into higher order modes which, moreover, attenuate faster than the fundamental mode. As already mentioned, the combination of these two aspects permits to achieve a quasi-single mode operation of the waveguide after a short propagation distance [44]. We set this condition to a modal purity value of the output of 95%, defined as the power fraction coupled to the fundamental mode compared to the total power distributed among all the relevant propagating modes (P_0/P_{tot}) [45].

In Fig. 7, as an example, the modal purity of the waveguide with d_c=12λ versus the propagation distance L and for different core height h is plotted. From this figure the propagation distances L^* at which the waveguide output reaches the value of P_0/P_{tot}=0.95 are L^*=3.66, 3.46 and 4.09 mm for h= 3λ, 5λ and 7λ, respectively.

In Table V are summarized the propagation distances L^* by varying d_c and h. Overall we found that the single mode operation requires propagation distances of only few millimetres. These values are smaller than those reported for hollow core fiber optics [45], allowing for the implementation of these waveguides in chip-scale format devices.

From Table V, the configuration that minimize L* corresponds to d_c=10λ and h=5λ. However, it must be highlighted that for long propagation distance L>>L* the higher order modes are essentially extinguished and the waveguide efficiency in terms of absolute output power is generally influenced by the coupling coefficient c_0 and the attenuation loss α_0 of the fundamental mode. As an example, from Table I and II the ratio between α_0 for d_c=10λ and d_c=12λ in the case of h=5λ is 1.64, while the ratio between c_0 is 1.08. Hence, the choice of the core size is a compromise between the requirements for single mode operation and the power output transmission efficiency. These considerations suggest that for h=5λ the waveguide with d_c=12λ provides better performance than the case with d_c=10λ at distances L>>L*.

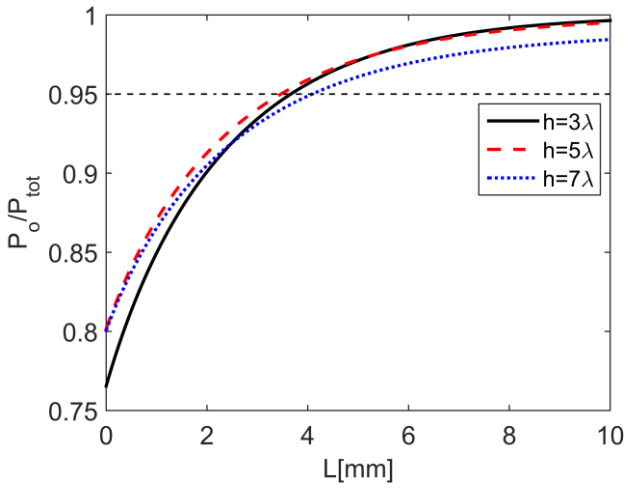

Fig. 7 Normalized power fraction coupled to the fundamental mode for d_c=12 λ versus L and for different core height h for a Si/SiO_2 SC-ARROW at the operating wavelength of λ=4μm.

TABLE V
L^*[MM]

h / d_c	3λ	5λ	7λ
10λ	1.81	1.35	1.81
12λ	3.66	3.46	4.09
14λ	6.48	6.62	7.41

B. Solid- cladding ARROW @9micron

From Fig. 4, the best performance at the operating wavelength of λ=9 μm are provided by the Si/AlN material composition for the cladding layers. In these case, taking into account the previous results, the waveguide modal analysis of the waveguide has been performed with h=5λ and by varying only the core width d_c =10λ, 12λ and 14λ.

TABLE VI
MODE ATTENUATION LOSSES α_0[CM^{-1}]

dc	α_0	α_{31}	α_{51}
10λ	0.55	1.24	11.40
12λ	0.34	1.02	6.67
14λ	0.24	1.60	4.23

By comparing the values of α_0 of Table VI and Table I we can observe an improvement of the performances of the waveguide in this configuration. These results are in very good agreement with those reported in section III (Fig.4).

To evaluate the waveguide modal purity in this case, a single mode fiber at λ=9 μm with a mode field diameter ($1/e^2$) of about 34 μm has been considered as the input in the EME simulations. In Fig. 8 the numerical results are plotted.

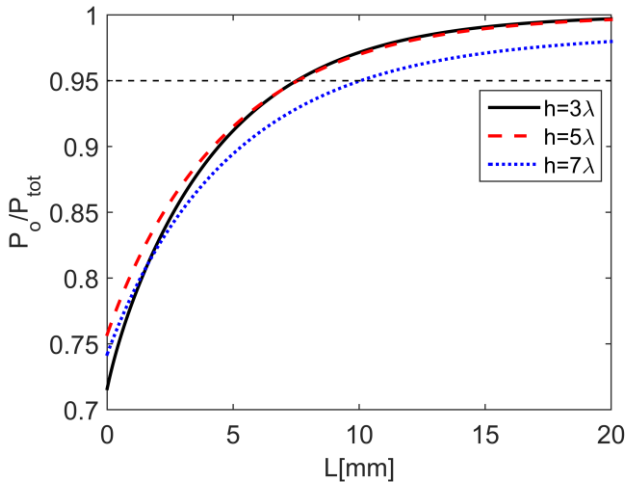

Fig. 8 Normalized power fraction coupled to the fundamental mode for d_c=12 λ versus L and for different core height h for a Si/AlN SC-ARROW at the operating wavelength of λ=9μm.

From this figure we have evaluated propagation distances of L^*=7.51, 7.56 and 10.05 mm for h= 3λ, 5 λ and 7λ, respectively.

V. Single Mode Analysis of SCH-ARROW

A stronger optical confinement in the hollow core is provided by using this waveguide geometry, thanks to the hollow claddings in the lateral structure that results in higher reflectivity mirrors. Since Silicon exhibits very low optical absorption in the IR range up to 14 μm, this configuration has been simulated at both the operating wavelength of λ=4 and 9 μm provided that the solid top- and bottom-claddings are accordingly selected.

At the operating wavelength of λ=4 μm, vertical confinement is obtained by employing solid claddings made-up of alternating Si/SiO_2 materials. SCH-ARROW with two bilayers has been simulated by varying the core width d_c and height h. The core size parameters considered in the simulations are d_c=8λ, 10λ and 12λ and h=3λ, 5λ and 7λ. The appropriate cladding layer thicknesses d_1 and d_2 have been calculated by using Eq. (1) with N=0 for each fixed core width d_c, except for the vertical silicon layer that has been calculated with N=1. This choice is related to the need to increase the mechanical stability of the structure and to simplify the fabrication manufacturing as the air trenches in the lateral structures can be produced with a single step etching process.

Table VII shows the calculated fundamental mode attenuation losses α_0 by varying d_c and h.

TABLE VII
FUNDAMENTAL MODE LOSSES α_0[CM^{-1}]

h / d_c	3λ	5λ	7λ
8λ	0.338	0.085	0.054
10λ	0.298	0.065	0.031
12λ	0.292	0.063	0.026

As expected, the waveguide performances are strongly improved with respect to the SC-ARROW, as the losses α_0 are reduced of about one order of magnitude.

In Fig. 9 is plotted the modal purity of the waveguide with $d_c=10\lambda$ versus the propagation distance L and for different core height h. From the figure, propagation distances of L^*= 2.33, 1.83 and 2.46mm have been obtained for h= 3λ, 5λ and 7λ, respectively.

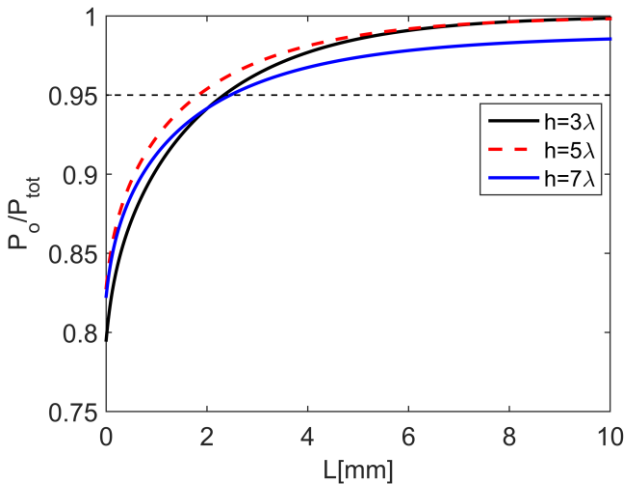

Fig. 9 Normalized power fraction coupled to the fundamental mode for $d_c=10\ \lambda$ for different core height h for a Si/SiO_2 SCH-ARROW at λ=4μm.

At the working wavelength of λ=9 μm, alternating Si/AlN materials have been chosen for solid top-and bottom-cladding layers. In this case, since the simulation domain became very large, we limit our attention to the configuration with $d_c=8\lambda$ and h=5λ due to memory size and computation time requirements. Very low attenuation loss of $\alpha_0=0.093\ cm^{-1}$ has been obtained with this configuration.

VI. CONCLUSION

In this paper, we report the design and the optimization for low-loss hollow core ARROW waveguide operating in the Mid-IR spectral range. In particular, we study two configurations for the waveguide, based on a conventional all solid claddings (SC-ARROW) and an innovative hybrid hollow/solid claddings (SCH-ARROW) structure. We propose a set of Si-CMOS compatible material compositions for these waveguides and presents the achievable optical performances. Moreover, in order to demonstrate the enormous potential offered by ARROW waveguides for the realization of common building blocks of photonic devices, we also report optimization criteria for single mode operation.

The study shows that the achievable propagation losses are competitive as compared with solid core waveguides and that the propagation length for single mode operation is of the order of few millimetres, depending on the operating wavelengths and core size. These results confirm that ARROW is a promising candidate for the implementation of high performances optical devices for gas sensing.

ACKNOWLEDGMENT

This research has been partially supported by the project IAMICA (Infrastructure of High Technology for Environmental and Climate Monitoring - PONa3_00363).

REFERENCES

[1] J. Hodgkinson and R. P. Tatam," Optical gas sensing: a review" *Meas. Sci. Technol.,* vol. 24, pp. 012004, 2013.
[2] T. Schädle and B. Mizaikoff, "Mid-Infrared Waveguides: A Perspective," *Appl. Spectrosc.*, vol. 70, pp.1625–1638, 2016.
[3] V. Singh et al., "Mid-infrared materials and devices on a Si platform for optical sensing," *Sci. Technol. Adv. Mater.*, vol. 15, no. 1, Art. no. 014603, 2014.
[4] T. Baehr-Jones, A. Spott, R. Ilic, A. Spott, B. Penkov, W. Asher, and M. Hochberg, "Silicon-on-sapphire integrated waveguides for the mid-infrared," *Opt. Express*, vol.18, pp. 12127-12135, 2010.
[5] A. Spott, Y. Liu, T. Baehr-Jones, R. Ilic, and M. Hochberg," Silicon waveguides and ring resonators at 5.5 μ m," *Appl. Phys. Lett.*, vol. 97, pp. 213501, 2010.
[6] F. Li et al., "Low propagation loss silicon-on-sapphire waveguides for the mid-infrared," *Opt. Express*, vol. 19, pp. 15212-15220, 2011.

[7] P. T. Lin, V. Singh, L. Kimerling, and A.M. Agarwal, “Planar silicon nitride mid-infrared devices,” *Appl. Phys. Lett.*, vol. 102, pp. 251121, 2013.

[8] J. Mu, R. Soref, L. C. Kimerling, and J. Michel, “Silicon-on-nitride structures for mid-infrared gap-plasmon waveguiding,” *Appl. Phys. Lett.*, vol. 104, pp. 031115, 2014.

[9] S. Khan, J. Chiles, J. Ma, and S. Fathpour,” Silicon-on-nitride waveguides for mid- and near-infrared integrated photonics,” *Appl. Phys. Lett.,* vol. 102, pp. 121104, 2013.

[10] E. Kasper, M. Kittler, M. Oehme, and T. Arguirov, "Germanium tin: silicon photonics toward the mid-infrared [Invited]," *Photon. Res.*, vol. 1, pp. 69-76, 2013.

[11] Y.-C. Chang, V. Paeder, L. Hvozdara, J.-M. Hartmann, and H. P. Herzig “Low-loss germanium strip waveguides on silicon for the mid-infrared,” *Opt. Lett.*, vol. 37, pp. 2883-2885, 2012.

[12] P. T. Lin, V. Singh, Y. Cai, L. C. Kimerling, and A. Agarwal, "Air-clad silicon pedestal structures for broadband mid-infrared microphotonics," *Opt. Lett.*, vol. 38, pp. 1031-1033, 2013.

[13] P. T. Lin et al. “Chip-scale Mid-Infrared chemical sensors using air-clad pedestal silicon waveguides,“ *Lab Chip*, vol. 13, pp. 2161-2166, 2013.

[14] Z. Cheng, X. Chen, C.Y. Wong, K. Xu and H. K. Tsang, “Mid-infrared suspended membrane waveguide and ring Resonator on Silicon-on-Insulator,” *IEEE Photon. J.*, vol. 4, pp. 1510-1519, 2012.

[15] B. J. Eggleton, B. Luther-Davies, and K. Richardson,”Chalcogenide photonics,” *Nat. Photonics*, vol. 5, pp. 141-148, 2011.

[16] P. Ma at al., "Low-loss chalcogenide waveguides for chemical sensing in the mid-infrared," *Opt. Express,* vol. 21, pp. 29927-29937, 2013.

[17] M. Sieger, et al, “On-Chip Integrated Mid-Infrared GaAs/AlGaAs Mach−Zehnder Interferometer,” *Anal. Chem.*, vol. 85, pp. 3050–3052, 2013.

[18] R. Shankar, I. Bulu, and M. Lončar,” Integrated high-quality factor silicon-on-sapphire ring resonators for the mid-infrared,” *Appl. Phys. Lett.*, vol. 102, pp. 051108, 2013.

[19] T. Hu, B. Dong, X. Luo, T. Liow, J. Song, C. Lee, and G. Lo, "Silicon photonic platforms for mid-infrared applications [Invited]," *Photon. Res.*, Vol. 5, pp. 417-430, 2017.

[20] J. S. Penadés, A. Z. Khokhar, M. Nedeljkovic, and G. Z. Mashanovich, “Low-loss mid-infrared SOI slot waveguides,” *IEEE Photon. Technol. Lett.*, vol. 27, pp. 1197–1199, 2015.

[21] P. St. J. Russell, P. Hölzer, W. Chang, A. Abdolvand, and J. C. Travers, “Hollow-core photonic crystal fibres for gas-based nonlinear optics,” *Nat. Photonics,* vol. 8, pp. 278-286, 2014.

[22] H. Schmidt and A. R. Hawkins. “Optofluidic Waveguides: I. Concepts and Implementations,” *Microfluid. Nanofluidics,* vol. 4, pp. 3-16, 2008.

[23] W. Yang, D. B. Conkey, B. Wu, D. Yin, A. R. Hawkins, and H. Schmidt, "Atomic spectroscopy on a chip," *Nat. Photonics*, vol. 1, pp. 331-335, 2007.

[24] T. Ritari, J. Tuominen, H. Ludvigsen, J. C. Petersen, T. Sørensen, T. P. Hansen, and H. R. Simonsen, “Gas sensing using air-guiding photonic bandgap fibers” *Opt. Express*, vol. 12, pp. 4080-4087, 2004.

[25] P. Patimisco, V. Spagnolo, M. S. Vitiello, G. Scamarci, C. M. Bledt, and J. A. Harrington, “Low-loss hollow waveguide fibers for mid-infrared quantum cascade laser sensing applications,” *Sensors*, vol. 13, pp. 1329-1340, 2013.

[26] A. Wilk, et al., “Substrate-integrated hollow waveguides: a new level of integration in mid-infrared gas sensing,” *Anal. Chem.*, vol. 85, pp. 11205-11210, 2013.

[27] J. J. R. Rohwedder, C. Pasquini, P. R. Fortes, I. M. Raimundo, A. Wilk and B. Mizaikoff, “iHWG-mNIR: a miniaturised near-infrared gas sensor based on substrate-integrated hollow waveguides coupled to a micro-NIR spectrophotometer,” *Analyst*, vol. 139, pp. 3572-3576, 2014.

[28] X. Fan and I. M. White, “Optofluidic microsystems for chemical and biological analysis,” *Nat. Photonics*, vol. 5, pp. 591-597, 2011.

[29] G. Testa, G. Persichetti, and R. Bernini, “Optofluidic approaches for enhanced microsensor performances,” *Sensors,* vol. 15, 465-484, 2015.

[30] G. Testa, G. Persichetti, and R. Bernini, “Liquid core ARROW waveguides: a promising photonic structure for integrated optofluidic microsensors” *Micromachines*, vol. 7, pp. 47, 2016.

[31] G. Testa, G. Persichetti, P.M. Sarro, and R. Bernini,“A hybrid silicon-PDMS optofluidic platform for sensing applications,” *Biomed. Opt. Express.*, vol. 5, pp. 417-426, 2014.

[32] D. Ozcelik, J.W. Parks, T.A. Wall, M.A. Stott, H. Cai, J.W. Parks, A.R. Hawkins, and H. Schmidt, "Optofluidic wavelength division multiplexing for single-virus detection", *PNAS*, vol. 112, pp. 12933-12937, 2015.

[33] R. Bernini, S. Campopiano, and L. Zeni, "Silicon micromachined hollow optical waveguides for sensing applications," *IEEE J. Sel. Topics Quantum Electron.*, vol. 8, pp. 106-110, 2002.

[34] G. Testa, C. Collini, L. Lorenzelli, and R. Bernini, “Planar silicon-polydimethylsiloxane optofluidic ring resonator sensors,” *IEEE Photon. Technol. Lett.*, vol. 28, pp. 155-158, 2016.

[35] H.P. Uranus, H.J.W.M. Hoekstra, and E. van Groesen, “Considerations on material composition for low-loss hollow-core integrated optical waveguides,” *Opt. Commun.*, vol. 260, pp.577-582, 2006.

[36] J. Lee, Z. Ye, K. Ho, and J. Kim, "Two-dimensional optofluidic liquid-core waveguiding based on optimized integration of single- and multiple-layer antiresonance reflection optical waveguides," *J. Opt. Soc. Am. B*, vol. 28, pp. 489-494, 2011.

[37] J. L. Archambault, R. J. Black, S. Lacroix and J. Bures, "Loss calculations for antiresonant waveguides," *J. Lightwave Technol.*, vol. 11, pp. 416-423, 1993.

[38] D. Yin, D.W. Deamer, H. Schmidt, J.P. Barber, and A.R. Hawkins, “Integrated optical waveguides with liquid cores,” *Appl. Phys. Lett.*, vol. 85, pp. 3477, 2004.

[39] J. Kischkat, S. Peters, B. Gruska, M. Semtsiv, M. Chashnikova, M. Klinkmüller, O. Fedosenko, S. Machulik, A. Aleksandrova, G. Monastyrskyi, Y. Flores, and W. Ted Masselink, "Mid-infrared optical properties of thin films of aluminum oxide, titanium dioxide, silicon dioxide, aluminum nitride, and silicon nitride," *Appl. Opt.*, vol. 51, pp. 6789-6798, 2012.

[40] T. Baba, Y. Kokubin, T. Sakaki and K. Iga, "Loss reduction of an ARROW waveguide in shorter wavelength and its stack configuration," *J. Lightwave Technol.*, vol. 6, pp. 1440-1445, 1988.

[41] Lin, P. T., Jung, H., Kimerling, L. C., Agarwal, A. and Tang, H. X., “Low-loss aluminium nitride thin film for mid-infrared microphotonics,” *Laser Photonics Rev.*, vol. 8, pp. L23–L28, 2014.

[42] R. Bernini, G. Testa, L. Zeni, and P. M. Sarro, "A 2 ×2 Optofluidic Multimode Interference Coupler," *IEEE J. Sel. Topics Quantum Electron.*, vol. 15, pp. 1478-1484, 2009.

[43] G Testa, Y Huang, PM Sarro, L Zeni, and R Bernini, “High-visibility optofluidic Mach–Zehnder interferometer”, *Opt. Letters*, vol. 35, pp. 1584-1586, 2010.

[44] G. Testa, G. Persichetti, and R. Bernini, “Design and optimization of an optofluidic ring resonator based on liquid-core Hybrid ARROWs,” *IEEE Photon. J.*, vol. 6, pp. 1-14, 2014.

[45] J. M. Kriesel, G. M. Hagglunda, N. Gat, V. Spagnolo, and P. Patimisco, “Spatial mode filtering of mid-infrared (mid-IR) laser beams with hollow core fiber optics,” *in Proc. SPIE*, vol. 8993, 89930V, 2014.

Dr Genni Testa received the Laurea degree (summa cum laude) in solid states physics from the University of Naples Federico II, Naples, Italy, in 2005, and the Ph.D. degree in electrical engineering from the Second University of Naples, Aversa, Italy, in 2008.

She is currently a researcher at the Institute for the electromagnetic sensing of the environment (IREA) of the Italian National Research council (CNR). Her research activities deal with the design, fabrication and characterization of microfluidic and optofluidic devices for biosensing and environmental applications. She is author or coauthor of more than 25 international journal papers and acts as a reviewer of several international journals.

Dr Gianluca Persichetti is a physicist. He received the Laurea degree at the University of Naples Federico II, Naples, Italy, in 2003 and the Ph.D. in "Novel Technologies for Materials Sensors and Imaging" in 2010 at the same University.

He is currently a researcher at the Institute for Electromagnetic Sensing of the Environment (IREA) of the National Research Council of Italy (CNR). His main research activities are the development of fiber optic sensors and spectroscopic sensors based on optofluidic waveguides.

Dr Romeo Bernini received his Laurea degree (summa cum laude) from the University of Naples Federico II, Naples, Italy, and his Ph.D. degree from the Second University of Naples, Aversa, Italy, in electronic engineering, in 1995 and 1999, respectively. He was a research fellow with the Second University of Naples in 2000. He is currently a senior researcher at the Institute for the electromagnetic sensing of the environment (IREA) of the Italian National Research council (CNR). His research fields are optoelectronic devices and sensors, microfluidic and optofluidic devices and fiber optic sensors. He has authored or coauthored more than 90 papers published in various international journals. He is a reviewer for several technical journals. He holds one international and two national patents on fiber optic sensors.